Surface segregation and effect of mechanical stress on Sb-stabilised tetragonal zirconia

Antonino Gulino,*[a] Russell G. Egdell,*[b] Giuseppe A. Baratta,[c] Giuseppe Compagnini[a] and Ignazio Fragalà*[a]

[a]*Dipartimento di Scienze Chimiche, Università di Catania, V.le A. Doria 6, 95125, Catania, Italy*
[b]*Inorganic Chemistry Laboratory, University of Oxford, South Parks Road, Oxford, UK OX1 3QR*
[c]*Osservatorio Astrofisico, Università di Catania, V.le A. Doria 6, 95125, Catania, Italy*

Compact pressure effects on Sb-doped tetragonal zirconia have been monitored using XRD, Raman and FTIR spectroscopies. A martensitic tetragonal→monoclinic transformation, driven by compact pressure, has been observed upon pelletisation of stabilised samples. By contrast, no monoclinic phase has been observed on amorphous powders upon pelletisation and firing. Sb surface segregation has been observed upon firing of pellets. The phenomenon has been quantitised by angle resolved XPS using the recent Gries algorithms to evaluate the Zr 3d photoelectron inelastic mean free path in ZrO_2 which, in turn, compares well with previous experimental data. Surface Sb segregation occurs over a depth range and involves many ionic planes. An experimental estimate of the Sb segregation enthalpy has been evaluated.

Partially stabilised tetragonal and fully stabilised cubic zirconia[1–6] have attracted considerable attention because of their remarkable physico-chemical properties.[2,7–16] Therefore, room-temperature stabilisation of highly symmetric polymorphs has been achieved by appropriate chemical substitution.

The mechanism of stabilisation of the tetragonal structure at room temperature has been widely investigated and several different arguments have been proposed.[2–5,17–32]

Tetragonal zirconia represents an important structural material due to the high melting point, low thermal conductivity, high strength and high fracture toughness[2,17,33] and finds many technological applications because of the enhanced properties.[5,17,33]

Fabrication procedures of ceramic zirconia specimens (bars, pellets, rods, *etc*.) use compacting pressure on powders even though stress-induced tetragonal-to-monoclinic (hereafter t→m) transformations have been observed and specimens with large monoclinic components become fragile.[17,33] In addition much attention has been devoted to the dependence of zirconia monoliths on processing procedures. Thus, mechanically induced zone darkening has been observed in stabilised zirconia composite materials.[5] Localised t→m transformation has been associated with deformation points and attributed to oxygen vacancy diffusion.[5] By contrast m→t transformation has also been observed either as a consequence of milling[17,21] or upon high pressure pelletisation (190 MPa) of as-sintered stabilised zirconia pellets.[34] Finally there is evidence that the martensitic t→m transformation involves a nucleation-controlled mechanism requiring large activation energies.[17] In this perspective there is a general consensus that crystallite grain sizes play a crucial role in stabilising zirconia ceramics and that small sizes favour tetragonal and cubic structures.[35–39]

In this wide context, it is worthy of mention that the electrical, mechanical and other technological properties of ceramic oxides are controlled to a large extent by segregation of impurities and dopants to surface and grain boundaries[40–42] and, therefore, that the structure and stability of the surface are largely governed by the dopant chemical environment. An adequate knowledge of the surface composition thus represents a crucial aspect for a full understanding of surface-related properties.

In the present paper, which complements a previous report on the ability of Sb ions to stabilise tetragonal ZrO_2,[37] we report on both the phase transformation of Sb-stabilised tetragonal ZrO_2 powders caused by compact pressure, as well as on the surface chemical composition of these materials.

Experimental

The Y-doped ZrO_2 (9 mol%) crystal (hereafter YSCZ) was obtained from ZIRMAT Corporation (MA, USA). Sb-doped ZrO_2 (3, 5, 10 and 15 mol%) powders were synthesised as previously described[37] and stepwise fired (24 h per step) at progressively higher temperatures ($\Delta T = 100\,^{\circ}C$), in the 200–1000 °C interval, in recrystallised alumina crucibles.

Pellets were obtained by pressing 1.5 g sample powders between 13 mm tungsten carbide dies (980 MPa) and firing for 24 h in recrystallised alumina boats. In particular, three different procedures have been adopted: firing of pressed amorphous sample powders, dried at 90 °C,[37] (pellet series *a*); pressing of fired (>400 °C) sample powders followed by a new firing (pellet series *b*); consecutive regrinding, in an agate mortar/pestle assembly, and repelletisation of pellets from series *b* followed by firing (pellet series *c*). No phase transformations were observed upon regrinding.

X-Ray diffraction (XRD) data were recorded on a computer interfaced Philips PW 1130 diffractometer as described elsewhere.[37]

Raman spectra were taken at 300 K using a JOBIN YVON U1000 double spectrometer equipped with a cooled photomultiplier and a photon counting chain. A 90° scattering geometry was used with 100 mW of output power on the 496.5 nm line coming from an Ar ion laser. The instrumental resolution was $2\,cm^{-1}$ with a 300 μm slits aperture.

Fourier transform IR reflectivity (FTIR) measurements were carried out, in the range 400–4000 cm^{-1}, with a Perkin-Elmer 1710 spectrometer. The resolution was $2\,cm^{-1}$ by using a DRIFT (diffuse reflectance) accessory by Spectra Tech. The collection angle is a fully π steradians, collecting 50% of the available diffuse energy and all of the reflected energy at a fixed 50° mean angle of incidence.

Doping levels of samples fired up to 1000 °C were quantitised by X-ray fluorescence (XRF) measurements as described elsewhere.[36,37,43]

Angle resolved X-ray photoelectron spectroscopy (ARXPS) measurements were made at different take-off angles (90, 80, 60, 45, 30, 15, 11, 9, 7, 5, 3, 1°) on sample powders and pellets with a PHI 5600 multi technique system (10^{-10} Torr regime).

Table 1 X-Ray fluorescence analysis and apparent atomic ratios from Sb $3d_{3/2}$ and Zr 3d core intensities in relevant ARXPS

nominal doping level (%)	firing temperature/°C	doping level from XRF (%)[a]	[Sb]/[Zr] from XPS[a] powder	pellet XPS take-off angle/degrees 1	3	5	9	30	45	90	surface Sb from eqn. (1); θ
3	800	2.80	0.14	0.16	0.16	0.16	0.15	0.15	0.14	0.13	0.14
5	800	4.48	0.24	0.27	0.24	0.23	0.22	0.22	0.20	0.18	0.21
10	500	9.38	0.12	0.18	0.18	0.18	0.18	0.18	0.18	0.18	0.18
10	800	9.35	0.34	0.40	0.40	0.39	0.39	0.38	0.37	0.34	0.29
10	1000	4.75	0.35	0.39	0.39	0.36	0.36	0.35	0.34	0.34	0.27
15	800	13.65	0.39	0.48	0.47	0.45	0.45	0.44	0.41	0.41	0.32

[a]Estimated uncertainities are $\pm 5\%$.

Resolution, correction for satellite contributions, background removal[44] and procedures to account for steady-state charging effect[45] have been described elsewhere.[36] To avoid *in situ* cleaning with ion bombardment, care was taken to introduce hot, furnace-annealed, ceramic discs.[41] In these conditions the remaining adventitious carbon surface contamination (284.6 eV binding energy) gave a measured C 1s/O 1s XPS intensity ratio of around 4/100. The O 1s core peak showed a single component, with no evidence of high binding energy shoulders due to water or hydroxide contamination.

Results and Discussion

XRF and XRD analysis

XRF data provide indications that all the samples stepwise fired up to 800 °C have final compositions close to the nominal values (Table 1). Higher firing temperatures (1000 °C) result in pronounced Sb loss (*ca.* 50%), possibly as Sb_4O_6 vapour[41,46] (Table 1).

The XRD patterns of all sample powders annealed up to 400 °C are typical of amorphous materials. In the 500–600 °C temperature range crystalline phases are formed. 5–15% doped samples show XRD peaks indicative of a tetragonal phase[37,47] still persisting up to 800 °C.[37] The splittings of XRD lines observed at 2θ *ca.* 35, 50 and 60° are fingerprints of tetragonal ZrO_2.[34,37,48] †

10% Sb-doped pellets in the series *a* [Fig. 1(*a*)] gave XRD patterns identical to those of unpressed powders (free of monoclinic phase).[37] By contrast, XRD patterns of pellets in the series *b* indicate the presence of both tetragonal and monoclinic phases [Fig. 1(*b*)].[47] In the series *c* [Fig. 1(*c*)] the intensity of lines associated with the monoclinic phase increases with a parallel fall-off of tetragonal reflections. No significant recovery of the tetragonal phase has been observed after prolonged further annealing. The fraction of monoclinic phase (M) in the pellets can be evaluated from the simple relationship:[49] $M = I_m(111)/[I_m(111) + I_t(111)]$ where $I_m(111)$ denotes the intensity of the monoclinic (111) peak and $I_t(111)$ refers to the intensity of the (111) tetragonal peak. Application of this criterion to 10% Sb-doped ZrO_2 fired at 800 °C indicates that pellets from series *b* and *c* contain 24 and 56% of the monoclinic phase, respectively. This is, therefore, evidence that the compacting pressure brings about a t→m transformation and that the effect is additive. Pellets in the series *a* do not undergo such an effect thus indicating that amorphous powders do not suffer any stress-induced t→m modification which precludes successive stabilisation upon annealing. This observation contrasts with that observed in many other systems. For example, as-sintered CeO_2–$YO_{1.5}$–ZrO_2 specimens, prepared from powders calcined at 500 °C, wet milled, dried and pelletised at low pressure (38–76 MPa) are almost purely monoclinic whereas higher pressure pelletised (190 MPa) specimens are tetragonal.[34] It has been reported that low compact pressure leaves behind a high porosity and hence favours monoclinic phase formation.[34] By contrast, the present data indicate that no monoclinic phase forms in the powders and that the quantity of monoclinic ZrO_2 in the pellets, made from powders calcined at $T > 400$ °C, does not change by varying the compact load in the range between 50 and 1000 MPa.

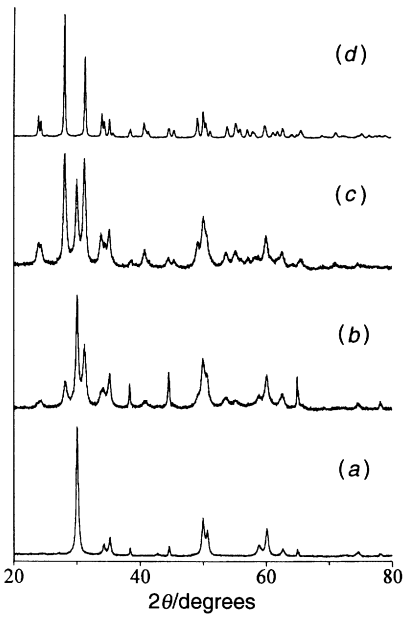

Fig. 1 X-Ray diffraction patterns, over the angular range $20° < 2\theta < 80°$, for 10% Sb-doped ZrO_2 samples: (*a*) pellets in series *a* fired stepwise at 800 °C; (*b*) pellets in series *b* fired stepwise at 800 °C; (*c*) pellets in series *c* obtained by regrinding and repelleting (5 times) pellets in series *b* and successively fired stepwise at 800 °C; (*d*) monoclinic pure ZrO_2. Peaks at $2\theta = 38.47°$, $2\theta = 44.73°$, $2\theta = 65.13°$ and $2\theta = 78.22°$ are due to the Al sample holder.

Raman and FTIR measurements

It has been already shown that Raman spectroscopy represents a powerful tool for a direct identification of crystal symmetry in zirconia polymorphs thus providing additional information to monitor phase transformations.[48,50,51]

The Raman spectrum of Y-stabilised cubic zirconia (YSCZ) consists of A_{1g}, E_{2g} and F_{2g} symmetry components[51] and resembles one-phonon density of states [Fig. 2(*a*)].[51] The band at *ca.* 610 cm^{-1} is dominated by the F_{2g} mode and minor A_{1g}, E_{2g} contributions are thus ignored.[51] Under uniaxial stress along the [001] and [111] directions, the frequency of the F_{2g}-type Raman band shifts linearly with the applied stress

† The splittings of the XRD lines observed in the present samples are: (002)–(200) at $2\theta \approx 35°$, (202) at $2\theta \approx 50°$ and (113)–(131) at $2\theta \approx 60°$.

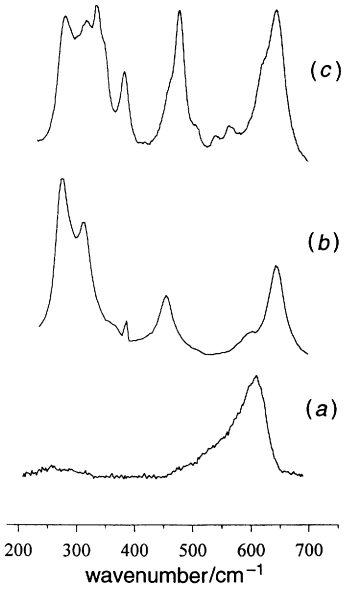

Fig. 2 Raman spectra of (*a*) 9% YSCZ crystal, (*b*) 10% Sb-doped ZrO_2 pellets in series *a* fired at 800 °C and (*c*) 10% Sb-doped ZrO_2 pellets in series *b* fired at 800 °C

and tends to increase with Y_2O_3 concentration. Polycrystalline yttria-stabilised tetragonal zirconia samples have been likewise studied.[48,50,51] They show six bands of symmetries $A_{1g}+2B_{1g}+3E_g$.[51] Their frequency shifts are generally smaller than those associated with cubic crystals.[51]

The Raman spectrum of a 10% Sb-doped zirconia pellet from series *a* [Fig. 2(*b*)] is a close counterpart of that previously reported for a Y-stabilised tetragonal zirconia (YSTZ) single crystal as expected for tetragonal ZrO_2.[51] In particular two bands are clearly visible at 645 cm^{-1} (E_g) and 604 cm^{-1} (A_{1g}). Pellets in the series *b* do not show the frequency shift associated with the E_g band at 645 cm^{-1} [Fig. 3(*c*)]. Nevertheless, the spectral profile is modified at lower frequencies and new bands appear at 563, 542 and 384 cm^{-1}, characteristic of the monoclinic symmetry.[50]

FTIR reflectance spectra (400–800 cm^{-1}) of pellets in the series *a* [Fig. 3(*a*)] show one broad Reststrahlen band around 480 cm^{-1}, which dominates the reflection spectrum, and a shoulder at 615 cm^{-1} superimposed on the high-frequency reflectivity. Values presently found agree well with corresponding values measured for YSTZ as expected for the tetragonal symmetry.[50] By contrast, two intense envelopes centred at 520 and 590 cm^{-1}, characteristic of the monoclinic phase, are also observed for pellets in the series *b* [Fig. 3(*b*)].[50] These observations agree well with XRD results and provide an indication that stress induces a t→m transformation in prestabilised tetragonal Sb-doped zirconia.

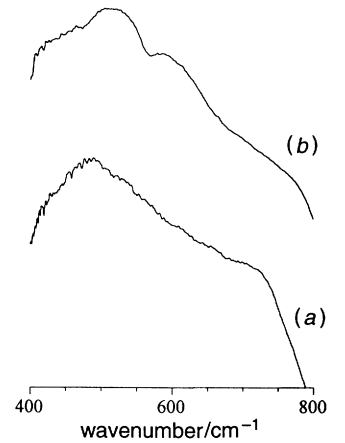

Fig. 3 FTIR spectra of (*a*) 10% Sb-doped ZrO_2 pellets in series *a* and (*b*) 10% Sb-doped ZrO_2 pellets in series *b*. Firing temperature = 800 °C.

Angle resolved XPS measurements

The relevant XPS feature of the 800 °C annealed Sb-doped ZrO_2 pellets from series *a* (45° take-off angle), consists of the main $3d_{5/2}$ and $3d_{3/2}$ spin–orbit components of Zr 3d core levels (181.8 and 184.1 eV, respectively).[37,52–55] Satellite features are also found at 15 eV higher binding energy (E_b), than Zr $3d_{5/2}$, due to shake-up processes.[53] In the 525–545 eV E_b region, the spectra of 5–15% Sb-doped ZrO_2 pellets in the series *a*, show (Fig. 4) almost totally overlapped Sb $3d_{5/2}$ and O 1s peaks. The Sb $3d_{3/2}$ peak is, therefore, left for quantitation of the surface Sb content[37,41,46] and Sb $3d_{3/2}$/Zr 3d intensity ratios have been used to evaluate the effective surface Sb/Zr atomic ratio making the due allowance for the relevant atomic sensitivity factors.[56] The values associated with different emission angles relative to the surface normal, are compiled in Table 1. It becomes evident both that (*i*) the intensity of the Sb 3d peaks is greater than would have been expected on the basis of the nominal doping levels, and that (*ii*) the Sb/Zr surface ratios suffer smaller changes than variations of nominal doping levels. Moreover, the enhanced Sb intensity at grazing emission angles, indicates different Sb concentration in the ionic layers probed by XPS.[41,46,57]

Consider now a series of cation-containing planes with interplanar separation *d*. Assuming that the top *n* layers have enriched dopant concentrations, it is possible to write a general expression for the angular variation of the XPS intensity ratio *I*(Sb 3d)/*I*(Zr 3d) corrected for the relevant atomic sensitivity factors,[41,58]

$$I(\text{Sb 3d})/I(\text{Zr 3d})=(\theta+xH_1)/[(1-\theta)+(1-x)H_2] \quad (1)$$

where $H_1=K_1/(1-K_1)$ and $K_1=\exp(-nd/\lambda_1 \sin\alpha)$ and $H_2=K_2/(1-K_2)$ and $K_2=\exp(-nd/\lambda_2 \sin\alpha)$.

Here λ_1 and λ_2 represent the photoelectron inelastic mean free path (IMFP) of Sb 3d and Zr 3d electrons respectively; x represents the nominal doping level; α is the photoelectron take-off angle relative to the surface plane; θ is the Sb occu-

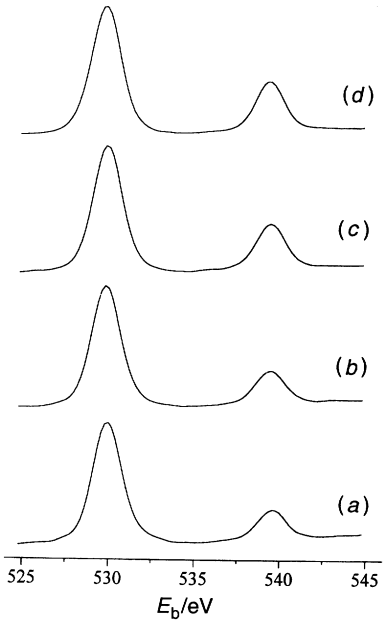

Fig. 4 Al-Kα excited normal emission XPS of 3–15% Sb-doped ZrO_2 pellets in series *a* fired at 800 °C and measured in the O 1s–Sb 3d binding energy region: (*a*) 3%; (*b*) 5%; (*c*) 10%; (*d*) 15% Sb. Structure due to satellite radiation has been subtracted from the spectra.

pancy of the Sb-enriched layers. A 2.96 Å value, corresponding to the separation between adjacent Zr-containing planes in the (111) direction,[47] has been taken for d.

The λ values have been estimated using the recent algorithm proposed by Gries[59]

$$\lambda = k_1(V_a/Z^*)E/[(\log_{10} E) - k_2] \quad (2)$$

where E is the energy of the analytical electron in eV; k_1 and k_2 are numerical fitting parameters (the former magnitude-adaptive, the latter energy-adaptive) derived from the optical IMFPs of Tanuma, Powell and Penn.[59] Z^* is a real number which can be regarded as the nominal 'effective' number of interaction-prone electrons per atom[59] and may be calculated: *viz.* $Z^* = (p\sqrt{Z_A} + q\sqrt{Z_B})/(p+q)$ for a given compound of stoichiometry A_pB_q and corresponding atomic numbers Z_A, Z_B; V_a is the atomic volume in cm^{-3} mol^{-1} which, for a compound of density ρ ($g\,cm^{-3}$) and mass numbers M_A, M_B, may be estimated from $V_a = (pM_A + qM_B)/\rho(p+q)$.

Taking $k_1 = 0.0019$ and $k_2 = 1.35$, the value of λ is given in units of nm.[59]

Using a ρ value of 6.05[33] $g\,cm^{-3}$, $\lambda_1 = 19$ Å and $\lambda_2 = 24$ Å are obtained for Sb 3d and Zr 3d core level peaks, respectively.

Ingo and Marletta have recently measured the effective XPS Zr 3d sampling depth in a 8% YSCZ crystal and values of 6.6 and 3.3 nm have been obtained at $\alpha = 90°$ and $\alpha = 30°$ photoelectron take-off angles, respectively.[60] Since the sampling depth is of the order of $3\lambda\sin\alpha$,[56] the value 6.6 nm corresponds to a λ value of 22 Å which is almost coincident with that obtained for Zr 3d by the Gries algorithm. The use of calculated values for Zr 3d and Sb 3d photoelectrons is however preferred because there is no empirical value for the IMFP of Sb 3d electrons in ZrO_2.

The intensity ratio I(Sb 3d)/I(Zr 3d) pattern, observed for the 800 °C annealed 10% Sb-doped ZrO_2 at different emission angles, is consistent with $\theta = 0.29$, assuming that the Sb enrichment is confined to the fifteen top-most ionic layers. Assuming $n = 15$, the increases of the Sb/Zr intensity ratio on going from 90 to 1° are in good agreement with the angular variation predicted by eqn. (1). By contrast, assuming that the enrichment involves a smaller number of ionic layers, each with an higher Sb occupancy, poorer agreement is obtained with the intensity ratio at grazing emission angles. Obviously, one limitation of the present approach lies in the use of a model which assumes a smooth (111) crystal surface to analyse experimental data obtained from a polycrystalline ceramic material.

It is worth noting that powders of 10% Sb-doped ZrO_2 annealed at 500 °C show a [Sb]/[Zr] ratio = 0.12, whilst pellets obtained from the same powder have $\theta = 0.18$. This result implies that compact pressure induces some segregation which is more evident at low annealing temperatures.

An experimental estimate of the segregation enthalpy of Sb in tetragonal Sb-doped ZrO_2 may be obtained by using the following expression:[41,61]

$$([Sb]/[Zr])_s = ([Sb]/[Zr])_b \exp(-\Delta_{segr}H/RT) \quad (3)$$

A plot of the natural logarithms of these ratios, in the present doping range, is given in Fig. 5. The cleaning procedure of the present samples has involved annealing at 800 °C followed by rapid cooling to room temperature and, hence, it is assumed that XPS probes equilibrium surfaces obtained at 800 °C. The value thus obtained for the heat of segregation is $\Delta_{segr}H = -0.677$ kJ mol^{-1}. The value depends on the bulk atomic ratio. Our value contrast with the positive heat of segregation observed by Hughes[57] for Y in 9.5% Y-doped ZrO_2, where $\Delta_{segr}H = 9.3 \pm 3.0$ kJ mol^{-1}. Moreover the current value is less negative than values observed in parent tetragonal systems (fired at 1000 °C), namely Sb-doped TiO_2 rutile ($\Delta_{segr}H = -2.380$ kJ mol^{-1}) and Sb-doped SnO_2 ($\Delta_{segr}H = -29.4$ kJ mol^{-1}).[41] Therefore, $\Delta_{segr}H = -0.677$ kJ mol^{-1} does not represent a surprisingly value since a large number of ionic planes are Sb-enriched.

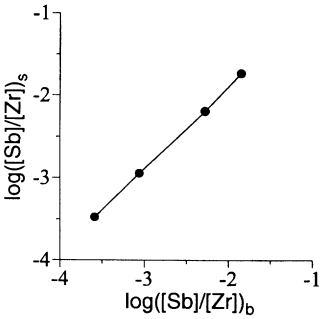

Fig. 5 Surface Sb 3d to Zr 3d intensity ratio plotted as a function of bulk doping level

Unfortunately, the possible presence of Sb in different oxidation states cannot be presently monitored since no chemical shifts are found between Sb^{III} and Sb^{V} ions. Indeed, in the mixed valence compound Sb_2O_4[62] a simple sharp peak is observed in the Sb $3d_{3/2}$ region and, similar to other post transition metal compounds, there is evidence that any intrinsic shift between Sb^{III} and Sb^{V} is balanced by the site potential difference for the two differing types of cations.‡

Conclusion

Effects of mechanical stress, driven by compact pressure during sample pelletisation, on 5–15 mol% Sb stabilised, air annealed (400–800 °C), ZrO_2 have been studied by XRD, Raman and FTIR measurements. Measurements on fired pellets upon pressing pre-calcined ($T > 400$ °C) tetragonal zirconia powders, indicate the presence of both tetragonal and monoclinic phases. This behaviour is a clear indication that compact pressure induces a t→m phase transformation. By contrast the absence of any monoclinic phase upon compact pressing of dried ($T = 90$ °C) amorphous powders, (5–15 mol% Sb) and subsequent firing (above 400 °C) is an indication that amorphous powders do not suffer any stress-induced modification. Angle resolved XPS measurements show both that progressive heat treatment of Sb-doped ZrO_2 causes surface Sb-segregation as well as that Sb enrichment involves many ionic layers.

Therefore these materials represent suitable candidates for precursors to solid state zirconia ceramics.

I. F. and A. G. thank the MURST and the CNR (Rome) for financial support.

References

1 A. F. Wells, *Structural Inorganic Chemistry 4*, Clarendon Press, Oxford, 1975.
2 P. Li, I-W. Chen and J. E. Penner-Hahn, *Phys. Rev. B*, 1993, **48**, 10063.
3 P. Li, I-W. Chen and J. E. Penner-Hahn, *Phys. Rev. B*, 1993, **48**, 10074.
4 P. Li, I-W. Chen and J. E. Penner-Hahn, *Phys. Rev. B*, 1993, **48**, 10082.
5 V. Sergo, C. Schmid, S. Meriani and A. G. Evans, *J. Am. Ceram. Soc.*, 1994, **77**, 2971.
6 K. Ishida, K. Hirota, O. Yamaguchi, H. Kume, S. Inamura and H. Miyamoto, *J. Am. Ceram. Soc.*, 1994, **77**, 1391.
7 T. H. Etsell and S. N. Flengas, *Chem. Rev.*, 1970, **70**, 1970.
8 K. Sasaki, H. P. Seifert and L. J. Gauckler, *J. Electrochem. Soc.*, 1994, **141**, 2759.
9 O. Yamamoto, Y. Arati, Y. Takeda, N. Imanishi, Y. Mizutani, M. Kawai and Y. Nakamura, *Solid State Ionics*, 1995, **79**, 137.

‡ For example, the Sn core binding energies of SnO and SnO_2 are identical.[63]

10 J. Van Herle, A. J. McEvoy and K. Ravindranathan Thampi, *J. Mater. Sci*., 1994, **29**, 3691.
11 H. Kurosawa, Y. Yan, N. Miura and N. Yamazoe, *Chem. Lett*., 1994, 1733.
12 G. Z. Cao, *J. Appl. Electrochem*., 1994, **24**, 1222.
13 K. Otsuka, T. Ando, S. Suprapto, Y. Wang, K. Ebitani and I. Yamanaka, *Catal. Today*, 1994, **24**, 315.
14 R. S. Garvie, R. H. Hannink and R. T. Pascoe, *Nature* (*London*) 1975, **258**, 703.
15 G. Fischer, *Ceram. Bull*., 1986, **65**, 1355.
16 T. Yokoyama, T. Setoyama, N. Fujita, M. Nakajima, T. Maki and K. Fuji, *Appl. Catal*., 1992, **88**, 149.
17 A. N. Scian, E. F. Aglietti, M. C. Caracoche, P. C. Rivas, A. F. Pasquevich and A. R. Lòpez Garcìa, *J. Am. Chem. Soc*., 1994, **77**, 1525.
18 P. Afanasief, C. Geantet and M. Breysse, *J. Mater. Chem*., 1994, **4**, 1653.
19 C. J. Norman, P. A. Goulding and I. McAlpine, *Catal. Today*, 1994, **20**, 313.
20 P. Afanasief and C. Geantet, *Mater. Chem. Phys*., 1995, **41**, 18.
21 E. Bailey, D. Lewis, Z. M. Librant and L. J. Porter, *Phase Transformation in Milled Zirconia*, *Trans. J. Br. Ceram. Soc*., 1972, **71**, 25.
22 P. Li, I-W. Chen and J. E. Penner-Hahn, *J. Am. Ceram. Soc*., 1994, **77**, 118.
23 J. Xue and R. Dieckmann, *Solid State Ionics*, 1994, **73**, 273.
24 M. Fukuya, K. Hirota, O. Yamaguchi, H. Kume, S. Inamura, H. Miyamoto, N. Shiokawa and R. Shikata, *Mater. Res. Bull*., 1994, **29**, 619.
25 S. Chen, W. Deng and P. Shen, *Mater. Sci. Eng. B*, 1994, **22**, 247.
26 M. M. R. Boutz, A. J. A. Winnubst, F. Hartgers and A. J. Burggraaf, *J. Mater. Sci*., 1994, **29**, 5374.
27 E. A. Van Arkel, *Physica*, 1924, **4**, 286.
28 S. M. Ho, *Mater. Sci. Eng*., 1982, **54**, 23.
29 M. Yoshimura, *Am. Ceram. Soc. Bull*., 1988, **67**, 1950.
30 J. Dexpert-Ghys, M. Faucher and P. Caro, *J. Solid State Chem*., 1984, **54**, 179.
31 J. G. Allpress and H. J. Rossell, *J. Solid State Chem*., 1975, **15**, 68.
32 A. Keshavaraja and A. V. Ramaswamy, *J. Mater. Res*., 1994, **9**, 837 and references therein.
33 R. A. Cutler, J. R. Reynolds and A. Jones, *J. Am. Chem. Soc*., 1992, **75**, 2173.
34 J. U. Wan and J. G. Duh, *J. Mater. Sci. Lett*., 1993, **12**, 575.
35 A. Chatterjee, S. K. Pradhan, A. Datta, M. De and D. Chakravorty, *J. Mater. Res*., 1994, **9**, 263 and references therein.
36 A. Gulino, S. La Delfa, I. Fragalà and R. G. Egdell, *Chem. Mater*., 1996, **8**, 1287.
37 A. Gulino, R. G. Egdell and I. Fragalà, *J. Mater. Chem*., 1996, **6**, 1805 and references therein.
38 A. Benedetti, G. Fagherazzi, F. Pinna and S. Polizzi, *J. Mater. Sci*., 1990, **25**, 1473.
39 B. J. Gould, I. M. Povey, M. E. Pemble and W. R. Flavell, *J. Mater. Chem*., 1994, **4**, 1815 and references therein.
40 R. G. Egdell and S. C. Parker, in *Science of Ceramic Interfaces*, ed. J. Nowotny, *Mater. Sci. Monogr*., Elsevier, Amsterdam, 1991, vol. 75, pp. 41–78.
41 A. Gulino, G. G. Condorelli, I. Fragalà and R. G. Egdell, *Appl. Surf. Sci*., 1995, **90**, 289 and references therein.
42 V. E. Henrich and P. A. Cox, *The Surface Science of Metal Oxides*, Cambridge University Press, Cambridge, 1994.
43 C. S. Hutchison, *Laboratory Handbook of Petrographic Techniques*, Wiley, New York, 1974.
44 M. Repoux, *Surf. Interface Anal*., 1992, **18**, 567.
45 G. M. Ingo, *Appl. Surf. Sci*., 1993, **70/71**, 235.
46 A. Gulino, A. E. Taverner, S. Warren, P. Harris and R. G. Egdell, *Surf. Sci*., 1994, **315**, 351.
47 American Society for Testing and Material, Powder Diffraction Files, Joint Committee on Powder Diffraction Standards, USA, 1974, Set 1–5 (Revised), Inorganic.
48 R. Srnivasan, S. F. Simpson, J. M. Harris and B. H. Davis, *J. Mater. Sci. Lett*., 1991, **10**, 352.
49 G. Gongyi and C. Yuli, *J. Am. Ceram. Soc*., 1992, **75**, 1294.
50 D. W. Liu, C. H. Perry and R. P. Ingel, *J. Appl. Phys*., 1988, **64**, 1413.
51 J. Cai, Y. S. Raptis and E. Anastassakis, *Appl. Phys. Lett*., 1993, **62**, 2781.
52 D. D. Sarma and C. N. R. Rao, *J. Electron. Spectr. Relat. Phenom*., 1980, **20**, 25.
53 G. Marletta and S. Pignataro, *Chem. Phys. Lett*., 1986, **124**, 414.
54 D. Majumdar and D. Chatterjee, *J. Appl. Phys*., 1991, **70**, 988.
55 F. Parmigiani, L. E. Depero, L. Sangaletti and G. Samoggia, *J. Electron. Spectrosc. Relat. Phenom*., 1993, **63**, 1.
56 D. Briggs and M. P. Seah, *Practical Surface Analysis*, Wiley, Chichester, 2nd edn., 1994.
57 A. E. Hughes, *J. Am. Ceram. Soc*., 1995, **78**, 369.
58 M. P. Seah, *Surf. Interface Anal*., 1980, **2**, 222.
59 W. H. Gries, *Surf. Interface Anal*., 1996, **24**, 38.
60 G. M. Ingo and G. Marletta, *Nucl. Instrum. Methods B*, 1996, **116**, 440.
61 L. Cao, R. G. Egdell, W. R. Flavell, K. F. Mok and W. C. Mackrodt, *J. Mater. Chem*., 1991, **1**, 785.
62 A. F. Orchard and G. Thornton, *J. Chem. Soc., Dalton Trans*., 1977, 1238.
63 C. Lau and G. K. Wertheim, *J. Vac. Sci. Technol*., 1978, **15**, 622.

Paper 7/00670E; *Received* 29*th January*, 1997